Flutter and Divergence Characteristics of Composite Plate Wing

M. Kassem Abbas[*], Hany M. Negm[†], M. Adnan Elshafei[‡]

Abstract: In the present work, an analytical investigation is introduced to determine the aeroelastic behavior of unswept, rectangular wings simulated by cantilevered composite plates using energy formulation and incompressible aerodynamic theory. Modified higher order shear deformation theory is used in the structural formulation. Doublet point method is used to solve the subsonic unsteady flow over the proposed rectangular wing. The flutter and divergence velocities are obtained using U-g method, which are validated by the analytical, finite element, wind tunnel test results available in the literature. The effect of composite fiber orientation on natural frequency, flutter and divergence speeds is discussed.

Keywords: Flutter, divergence, aeroelasticity, composite plate, unsteady aerodynamic, doublet point method, energy method

1. Introduction

Aeroelastic phenomena happen due to the interactions of the inertial force, elastic force and aerodynamic load. Flutter increases the amplitude of vibration which causes high cyclic stresses and failure of the wing. Divergence also may quickly develop into catastrophic torsional structural failure. Many researchers introduced several models to investigate flutter and divergence phenomena of airplane wings.

Hollowell et al. [1], 1984, investigated, analytically and verified experimentally, the modeling of the aeroelastic behavior of unswept rectangular wings simulated by graphite/epoxy plates with various amounts of bending- torsion stiffness coupling. The analytical approach incorporated a Rayleigh-Ritz energy formulation and an unsteady, incompressible two-dimensional aerodynamic theory. Flutter and divergence velocities were obtained using the U-g method and compared to the results of low speed wind tunnel tests. They concluded that wings with negative stiffness coupling exhibit divergence, while positive coupling delayed the occurrence of stall flutter.

Lin et al. [2], 1989, used a 18-degree-of freedom triangular plate finite element. They studied the effects of composite fiber angle, orthotropic modulus ratio, sweep angle, and aspect ratio on the vibration, flutter, and divergence characteristics of cantilever plates in subsonic flow. The stiffness and mass matrices are generated according to the classical lamination theory. The unsteady air load is evaluated using lifting surface theory, solved numerically by doublet-lattice method. Interpolation using a surface spline is employed to interconnect the structural nodal and aerodynamic control points. They concluded that effective enhancement of flutter/ divergence performance can be attained by varying the orthotropic modulus ratio when an

---
[*] Egyptian Armed Forces, Egypt.
[†] Department of Aerospace Engineering, Cairo University, Cairo, Egypt.
[‡] Egyptian Armed Forces, Egypt; maelshafei@yahoo.com .

appropriate fiber orientation is selected. They found also that structural tailoring can provide a harmonious balance to the sweep angle effect upon the aeroelastic stability characteristics of a wing.

Koo et al. [3], 1994, investigated structural damping effect on the flutter boundary for three types of composite wings: rectangular, swept-forward, and swept-back using the finite element technique. The unsteady aerodynamic loads on oscillating wings are evaluated by doublet point method. The interpolation between the structural and aerodynamic grids is accomplished by using surface splines. The effects of fiber orientation on the flutter/ divergence characteristics were investigated. They concluded that the structural damping of composite materials increases the flutter speeds and decreases the flutter frequencies.

Wael [4], studied the static and dynamic aeroelastic behavior of composite swept wings using a modified approach based on the equivalent plate concept using classical and first order plate theories. He made a parametric study to illustrate the effect of wing aspect ratio, taper ratio, sweep angle, number of layers, and fiber orientations on the divergence, control reversal, and flutter phenomena. He concluded that wing's divergence speed can be improved by moving the principal skin stiffness direction ahead of the wing reference axis. Similarly, flutter characteristics of sweep back wings can be improved by moving the principal skin stiffness direction behind the wing reference axis.

Dunn et al. [5], 1992, investigated the nonlinear stalled aeroelastic behavior of rectangular graphite/epoxy cantilevered wings with varying amounts of bending-torsion stiffness coupling. A wind-tunnel test was performed to validate the analytical model.

Livne [6], 1995, used equivalent plate structural modeling and doublet point lifting surface unsteady aerodynamics to obtain analytic sensitivities of aeroservoelastic response with respect to wing and control surface planform shape parameters. He developed an efficient approximation technique for wing shape optimization as a multidisciplinary optimization strategy.

Lu et al. [7], 1992, presented a theoretical analysis of the flutter suppression of oscillating thin airfoils using active acoustic excitations in incompressible flow. Closed-form unsteady aerodynamic loads induced by a simple harmonic acoustic excitation on a typical section model are derived. The flutter boundaries of the typical section were evaluated using both the U-g and root locus methods.

Many methods have been developed for calculating the unsteady pressure distribution on a thin finite wing in subsonic flow since Kussner [8], formulated the governing integral equation. The methods can be divided into two principal categories, the mode function method and the direct element method. Watkins et al. [9], developed the mode function method for practical use. Rowe et al. [10], calculated successfully the unsteady pressure distribution on wings with control surfaces.

A typical procedure of the discrete-element method type is the doublet lattice method [11-13]. This method is used widely because of its ready applicability to complex wing configurations. Although the method yields reasonable results, it contains an inconsistency in the steady-state part. It must be calculated with the aid of the vortex lattice method despite the fact that the basic equation of doublets is valid even when the flow becomes steady, [11].

Ueda et al. [14], developed a simple method for calculating unsteady aerodynamic loads on harmonically oscillating thin wings in subsonic flow. Their doublet point method is based on a concept of concentrated lift forces. The wing is divided into element surfaces on which the lift distribution is represented by single concentrated lift forces. This method is explained and applied in the present work.

Modified higher order shear deformation theory (MHSDT) [15], is used to formulate the equation of motion of the composite wing. Unsteady aerodynamic loads on harmonically oscillating thin wings in subsonic flow are calculated. The doublet point method is used, based on a concept of concentrated lift forces, to solve the subsonic unsteady flow over a

rectangular wing. Flutter and divergence velocities are obtained using U-g method and compared to the published analytical, finite element, and wind tunnel test results available in the literature.

2. Structural Formulation

The wing is idealized by a rectangular cantilevered composite plate with uniform thickness. The transverse deflection equation, written in generalized coordinates, is

$$w_0(x,y,t) = \{a_3(x,y)\}^T \{q_3(t)\} \tag{1}$$

where $\{a_3(x,y)\}$ is the column vector of the Ritz approximation functions that satisfy the cantilever plate boundary conditions as given by Kassem et al. [15],

$$\{a_3(x,y)\}^T = \begin{bmatrix} x^2 & x^2y & x^3 & x^2y^2 & x^3y & x^4 & x^3y^2 & x^4y & x^4y^2 \end{bmatrix}_{1x9} \tag{2}$$

$\{q_3(t)\}$ is the column vector of Ritz coefficients, which are the unknowns of the structural problem. Using Hamilton's principle, the system of equations of motion is obtained as given by Kassem et al. [15]:

$$[M]\{\ddot{q}\} + [K]\{q\} = \{F_{z0}\} \tag{3}$$

where $[K]$ and $[M]$ are the stiffness and mass matrices, $\{F_{z0}\}$ is the concentrated load vector representing the aerodynamic load distribution on the wing, calculated using doublet point method. $\{q\}$ is the generalized coefficient vector to be determined.

3. Unsteady Aerodynamic Formulation (Doublet Point Method)

The doublet point method is used to calculate the subsonic unsteady aerodynamic forces which act on two-dimensional wings. The aerodynamic loads are calculated as concentrated loads, which make the concentrated load vector $\{F_{z0}\}$, the right hand side of the equations of motion, Eq.(3). Results obtained by the method can easily be combined with aeroelastic analysis to calculate flutter and divergence velocities.

The pressure distribution on oscillatory lifting surfaces and its corresponding upwash velocity distribution are related by the integral equation, [8, 14, 16],

$$v_I(x,y) = \frac{1}{8\pi} \iint_S \Delta p(\xi,\eta) K(x_0,y_0) d\xi d\eta \tag{4}$$

The lifting surface is assumed to lie in the x-y plane (z = 0), where S denotes the region of the wing area, and the nondimensional pressure distribution Δp is defined by

$$\Delta p = \frac{p'_+ - p'_-}{\frac{1}{2}\rho_\infty u_\infty^2} \tag{5}$$

where p'_+ and p'_- are the disturbance pressure on the upper and lower surfaces of the wing, respectively. The denominator on the right-hand side of Eq.(5) is the dynamic pressure of the uniform flow, and the Kernel function $K(x_0,y_0)$ in Eq.(4) can be written as

$$K(x_0,y_0) = e^{-ikx_0}\left[\frac{Me^{ikx}}{R\sqrt{X^2+r^2}} + B(k,r,X)\right] \tag{6}$$

Parameters used in the Eq.(6) are defined in Appendix (A), [14].

Since the kernel function $K(x_0, y_0)$ corresponds to a normal velocity field that is produced by a point doublet of the acceleration potential located at (ζ, η), it is called a doublet point. The point (x, y) is called an upwash point where the normal velocity of the upwash is placed. The wing planform is divided into panel segments called element surfaces. Each element surface is constructed such that the two side edges are parallel to the uniform flow. We identify the individual elements by numbering them from 1 to N, Fig. 1.a.

(a)

(b)
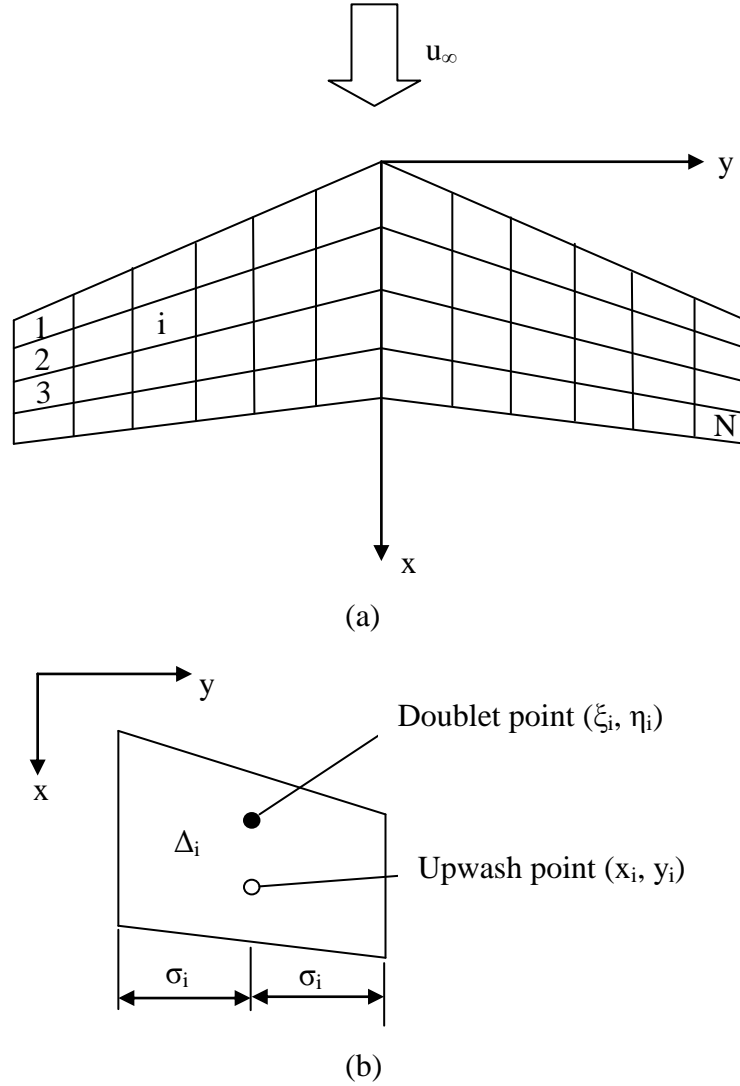
Fig. 1. Aerodynamic elements in doublet point method, [14]

Fig. 1.b shows a focus on the ith element surface. The trapezoid of the element has an area Δ_i, and width $2\sigma_i$. Using the $\frac{1}{4} - \frac{3}{4}$ chord rule for element surfaces, the lift distribution on the surface is concentrated at the point (ζ_i, η_i) on the quarter chord at the midspan of the element (i). Thus, the location (ζ_i, η_i) is the doublet point of the element surface (i). The upwash of the three-quarter chord point (x_i, y_i) at the midspan is taken as representative of the whole upwash distribution on the element surface (i). These assumptions make it possible to discretize the integral in Eq.(4) into linear algebraic equations. Instead of Eq.(4), the upwash w_i of the ith element can be calculated in a discrete form as [14]:

$$v_I(x_i, y_i) = \frac{1}{8\pi} \sum_{j=1}^{N} \Delta p(\xi_j, \eta_j) \Delta_j K(x_i - \xi_j, y_i - \eta_j), \quad (i = 1...N) \tag{7}$$

Eq.(7) can be expressed in a matrix form, as follows:

$$\{v_I\} = [D].\{c_p\} \tag{8}$$

where $\{v_I\}$ is the induced velocities at the elements' upwash points (x_i, y_i), $[D]$ is the matrix of aerodynamic influence coefficients, and $\{c_p\}$ is the pressure coefficient vector which represents the pressure coefficient at each element's doublet point, Fig. 1.b, defined as follows:

$$v_I = \{v_{Ii}\} = \{v_I(x_i, y_i)\} \tag{9}$$

$$D = [d_{ij}] = \frac{\Delta_j}{8\pi} K(x_i - \xi_j, y_i - \eta_j) \tag{10}$$

$$c_p = \{c_{p_j}\} = \{\Delta p(\xi_j, \eta_j)\} \tag{11}$$

The upwash vector $\{v_I\}$ is calculated for element (i) using the following form, [14]:

$$v_{I_i} = \frac{\partial}{\partial x} w_0(x_i, y_i) + i k w_0(x_i, y_i) \tag{12}$$

where $w_0(x_i, y_i)$ is the mid-plane (z=0) vertical displacement at the upwash point (x_i, y_i) of element (i).

Solving Eq.(8), we can directly obtain the unsteady aerodynamic pressure coefficient distribution at the doublet point of each element area. When the reduced frequency k tends to zero the flow becomes steady. The complex lift and moment coefficients can be calculated as mentioned in Appendix (B).

Using the transverse deflection equation, Eq. (1), the induced velocity can be written as,

$$v_{I_i} = ([v_{IR}]_i + i[v_{II}]_i).\{q_3\}$$

$$[v_{IR}]_i = \left\{ \frac{\partial a_3}{\partial y}(x_i, y_i) \right\}^T \tag{13}$$

$$[v_{II}]_i = k\{a_3(x_i, y_i)\}^T$$

The induced velocities of all elements can be written in vector form as,

$$\{v_I\} = [v_{IT}].\{q_3\}$$
$$[v_{IT}] = [v_{IR}] + i[v_{II}] \tag{14}$$

where the dimensions of the induced velocity vector $\{v_I\}$ are $N_e \times 1$, and the dimensions of $[v_{IR}]$ and $[v_{II}]$ are $N_e \times 9$, where N_e is the total number of aerodynamic elements. Substituting into Eq.(8), the unsteady aerodynamic pressure coefficient distribution c_p on the plate wing can be written as:

$$\{c_p\} = [D]^{-1}[v_{IT}].\{q_3\} \tag{15}$$

The transverse aerodynamic load at element (i) can be obtained by,

$$F_{ai} = \frac{1}{2} \rho U^2 S_i c_{p_i} \tag{16}$$

where ρ is the air density, U is the uniform flow speed, and S_i is the area of element (i). The transverse load vector of all elements can be written as,

$$\{F_a\} = \frac{1}{2}\rho U^2 [S]\{c_p\} \qquad (17)$$

$[S]$ is a square diagonal matrix consisting of the elements areas. Substituting Eq.(15),

$$\{F_a\} = \frac{1}{2}\rho U^2 [Ar].\{q_3\} \qquad (18)$$

where $[Ar]$ is a matrix of dimensions $N_e \times 9$ defined as follows:

$$[Ar] = [S][D]^{-1}[v_{IT}] \qquad (19)$$

Due to symmetry, the transverse aerodynamic loads applying on the half wing only are taken into consideration. Using the energy method, the concentrated load vector in the transverse z-direction applied at the doublet point of element (i) is, [15]:

$$\{F_{z0}\}_i = F_{zi}\{a_3(\zeta_i, \eta_i)\} \qquad (20)$$

where (ζ_i, η_i) is the coordinates of the doublet point of element (i), Fig. 1.b. The concentrated load vector in the transverse z-direction applied at the half wing can be written in matrix form as:

$$\{F_{z0}\} = \sum_{i=1}^{N_e/2}\{F_{z0}\}_i = [a_3]\{F_a\} \qquad (21)$$

where $[a_3]$ is a matrix of dimensions $9 \times (N_e/2)$ including columns of Ritz approximation functions, (2), obtained by substituting in column (i) for x and y with ζ_i and η_i of element (i) from $i = 1$ to $N_e/2$. Substituting for $\{F_a\}$ from Eq.(18),

$$\{F_{z0}\} = \frac{1}{2}\rho U^2 [a_3][Ar].\{q_3\} \qquad (22)$$

This is the final form of the transverse load vector applied on the half wing due to unsteady aerodynamics using the doublet point method. It is important to note that the applied aerodynamic load is a function of the column vector of Ritz coefficients $\{q_3(t)\}$, which represent the time-dependent transverse deflection of the mid-plane of the cantilever plate. Using Eq.(22), the equations of motion of the wing can be written as,

$$[M_w]\{\ddot{q}_3\} + [K_w]\{q_3\} = \frac{1}{2}\rho U^2 [a_3][Ar].\{q_3\} \qquad (23)$$

where $[M_w]$ and $[K_w]$ are the mass and stiffness sub-matrices corresponding to the transverse deflection with dimensions 9×9 taken from the global mass and stiffness matrices derived in [15].

4. Flutter Analysis

Assuming harmonic (sinusoidal) motion, $\{q_3(t)\}$ can be expressed as,

$$\{q_3\} = \{\bar{q}_3\}e^{i\omega t} \qquad (24)$$

Hence

$$\{\ddot{q}_3\} = -\omega^2\{\bar{q}_3\}e^{i\omega t} \qquad (25)$$

where $\{\bar{q}_3\}$ is the amplitude of the column vector of Ritz coefficients, ω is the oscillation frequency. Define the reduced frequency k, [17],

$$k = \frac{\omega b}{U} \tag{26}$$

Substituting from Eq.(24) and Eq.(26), the equation of motion Eq.(23) can be rearranged to the form,

$$[K_w]\{\bar{q}_3\} - \omega^2 ([M_w] + [\bar{A}])\{\bar{q}_3\} = 0 \tag{27}$$

where $[\bar{A}]$ represents the aerodynamic matrix:

$$[\bar{A}] = \rho \frac{b^2}{2k^2}[a_{3R}][Ar_R] \tag{28}$$

The flutter analysis can be performed using the U-g method, [17]. The structural damping coefficient (g) is introduced in the equations of motion, representing the amount of damping that must be added to the structure to attain neutral stability (flutter) at the given velocity, [1]. Negative values of structural damping (g) indicate that the structure is stable, while positive values indicate instability. Flutter occurs when the structural damping coefficient (g) equals zero. From Eq.(27), the following eigenvalue problem can be written,

$$((1+ig)[K_w] - \omega^2([M_w] + [\bar{A}]))\{\bar{q}_3\} = 0$$
$$(Z[K_w] - [\bar{B}])\{\bar{q}_3\} = 0 \tag{29}$$

where

$$[\bar{B}] = [M_w] + [\bar{A}] \tag{30}$$

$$Z = \frac{(1+ig)}{\omega^2} \tag{31}$$

For a given value of reduced frequency, k, the complex aerodynamic matrix, $[\bar{A}]$, is evaluated using Eq.(28), and together with $[M_w]$ and $[K_w]$ are placed into Eq.(29), which is solved for the complex eigenvalues Z. From these eigenvalues and from given k, the frequency (ω), the structural damping coefficient (g), and the corresponding speed (U) are determined as flows,

$$\omega = \sqrt{\frac{1}{Z(\text{Re})}}, \qquad g = \frac{Z(\text{Im})}{Z(\text{Re})}, \qquad U = \frac{\omega b}{k} \tag{32}$$
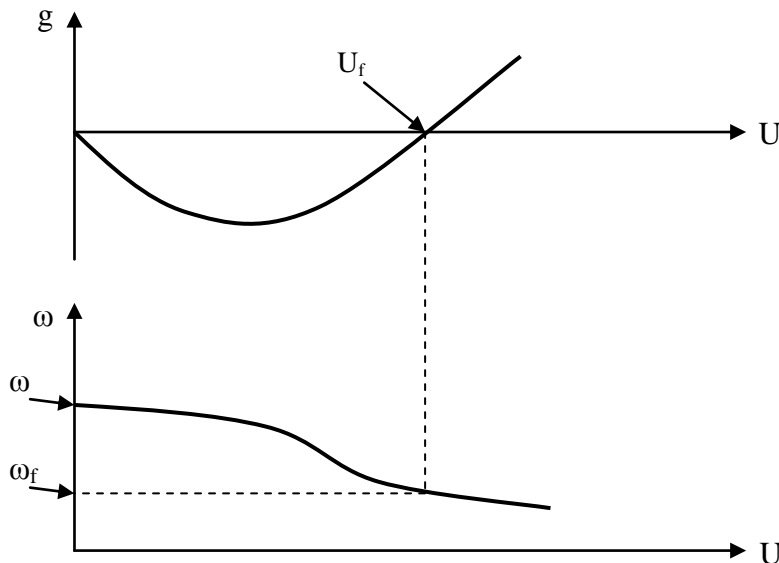
Fig. 1. U-g and U-ω curves to find flutter speed (U$_f$) and flutter frequency (ω$_f$)

A Plot of g and ω vs. U characterize the flutter stability and frequencies of the wing. The ω values at $g \sim 0$ represents the flutter frequency, Fig. 1, [1].

5. Divergence

The divergence speed (U_D) can be calculated directly by neglecting the mass matrix $[M_w]$ in Eq.(27), and rearranging equations into the form

$$\left(\left[\bar{A}_{stat} \right] - \lambda \left[K_w \right] \right) \{ \bar{q}_3 \} = 0 \tag{33}$$

where the static aerodynamic matrix $\left[\bar{A}_{stat} \right]$ has now all real coefficients, and is represented by,

$$\left[\bar{A}_{stat} \right] = \lim_{k \to 0} \frac{1}{2} \rho \left[a_{3R} \right] \left[Ar_R \right] \tag{34}$$

and the eigenvalue λ represents;

$$\lambda = \frac{1}{U_D^2} \tag{35}$$

The largest positive eigenvalue λ gives the lowest divergence speed U_D.
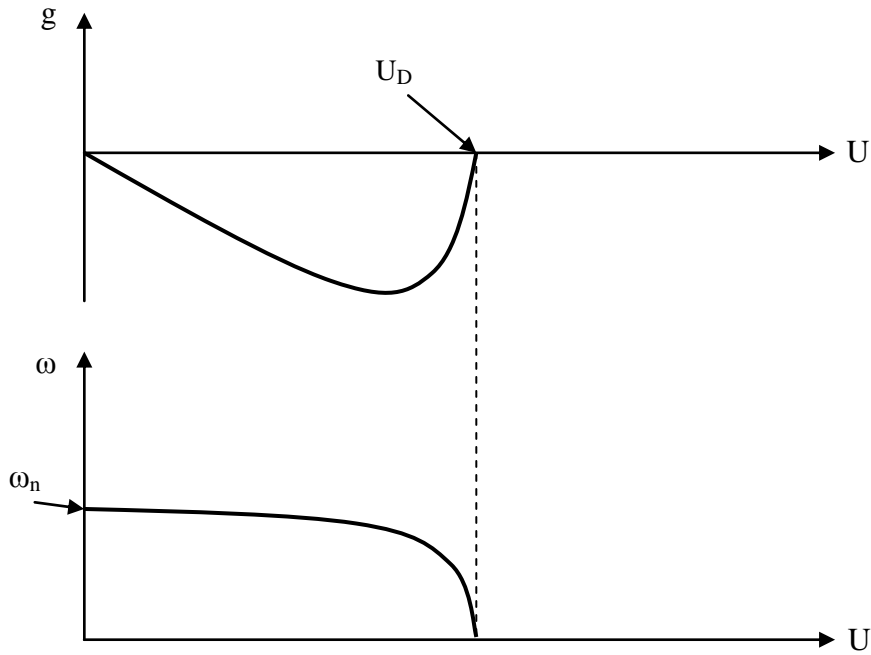
Fig. 1. U-g and U-ω curves to find divergence speed (U_D)

6. Numerical Results and Discussion

The aerodynamic and aeroelastic theories are first verified, then a parametric aeroelastic study is performed. A MATLAB code for the used doublet point method is developed and verified on a rectangular wing in steady and unsteady flow. The pressure distribution, lift coefficient, and moment coefficient are calculated and compared with the published data. Then the flutter and divergence performance of a rectangular composite plate is calculated and verified with the available published data. Finally, the effect of composite fiber orientation on natural frequency, flutter and divergence speeds is discussed.

6.1. Aerodynamics of Rectangular Wing in Steady flow

A rectangular wing of aspect ratio AR=2 in steady flow ($k \to 0$) is discussed. The wing rotates around its mid-chord with angle of attack (α). The pressure distribution and the lift coefficient slopes have been calculated for various numbers of elements as shown in Fig. 1, Fig. 2 and Fig. 3. The chord pressure distributions at the location y=0.2 is shown in Fig. 2 for three different chordwise numbers of elements N_x. The spanwise number of elements is fixed at five. It can be seen from the figure that even a small number of elements gives satisfactory results. The convergence with the spanwise number of elements is shown in Fig. 3 with a fixed chordwise number of elements. Lift and moment coefficients are calculated as mentioned in Appendix (B).
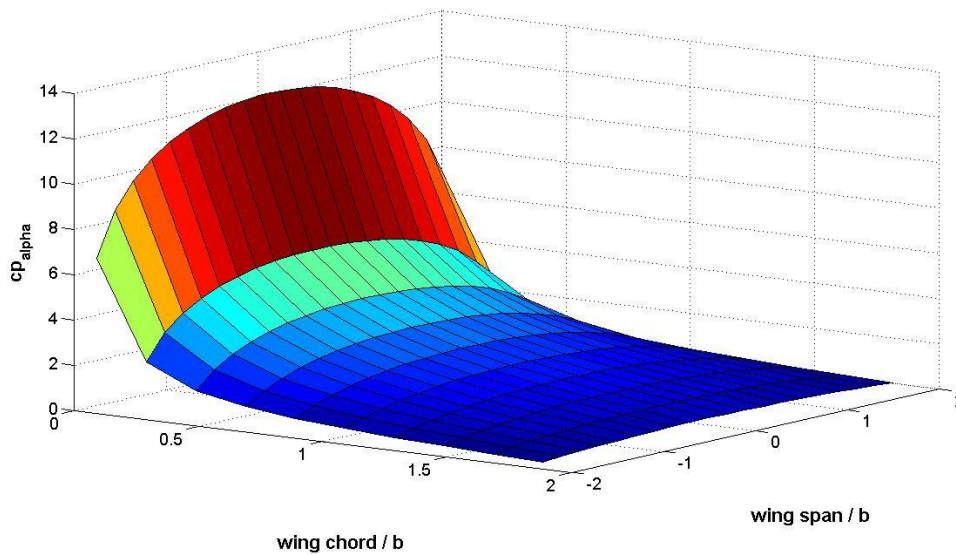
Fig. 1. 3-D pressure distribution on a rectangular wing (AR=2, k=0, M=0, N_x=10, N_y=10)
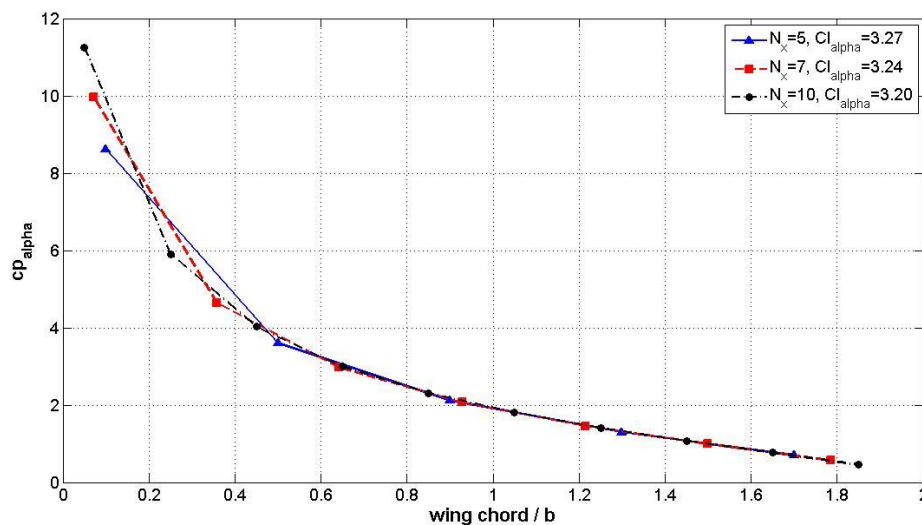
Fig. 2. Chordwise pressure coefficient slope distribution of a rectangular wing at station y=0.2 (AR=2, k=0, M=0, N_y=10)
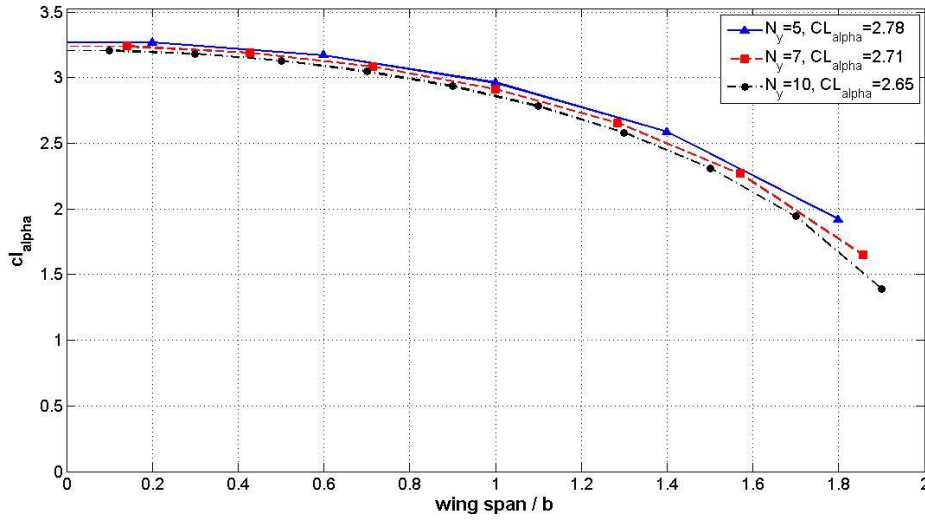
Fig. 3. Spanwise lift coefficient slope distribution of a rectangular wing (AR=2, k=0, M=0, N_y=10)

6.2. Aerodynamics of Rectangular Wing in Unsteady Flow

Rectangular wing of aspect ratio (AR 2) is calculated in unsteady flow. The wing oscillates in pitching around its mid-chord with angle of attack (α). The real and imaginary parts of the pressure distribution are shown in Fig. 4 and Fig. 5, respectively. The real and imaginary parts of the lift coefficient slope c_{l_α} span-wise distributions are shown in Fig. 6 and Fig. 7, respectively. The real and imaginary parts of the pressure coefficient c_{p_α} chordwise distributions at the tip and root of the considered wing are shown in Fig. 8 and Fig. 9, respectively. Fig. 10 presents the magnitude of the complex lift and moment coefficients C_L and C_M vs. reduced frequency (k). Fig. 11 presents the phase of the complex lift and moment coefficients C_L and C_M vs. reduced frequency. Lift and moment coefficients are calculated as mentioned in Appendix (B). All the presented results are compared to the available published data, [14]. Good correlation is shown.
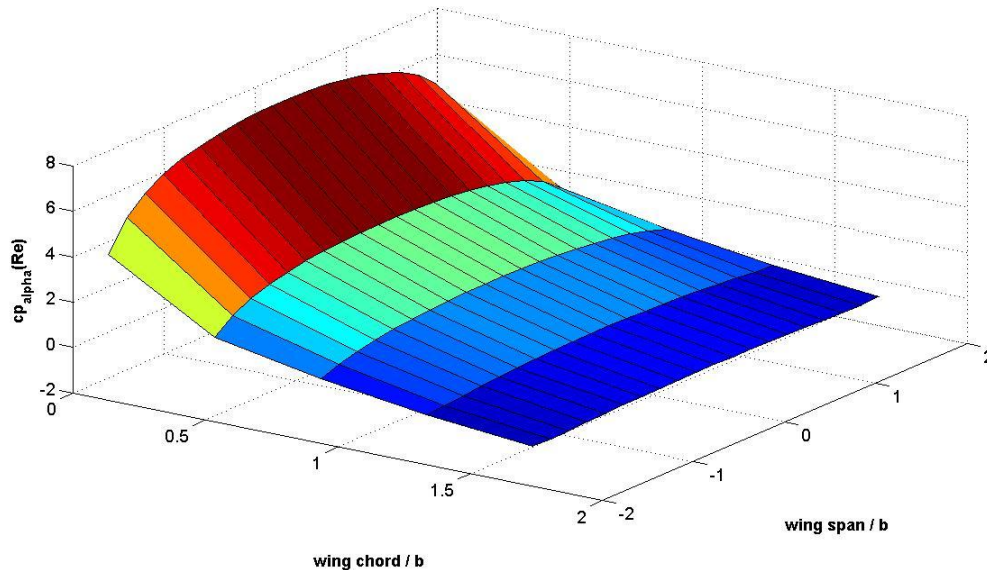
Fig. 4. Real part of the pressure distribution on a rectangular wing oscillates in pitching motion (AR=2, k=1, M=0, N_x=5, N_y=10)
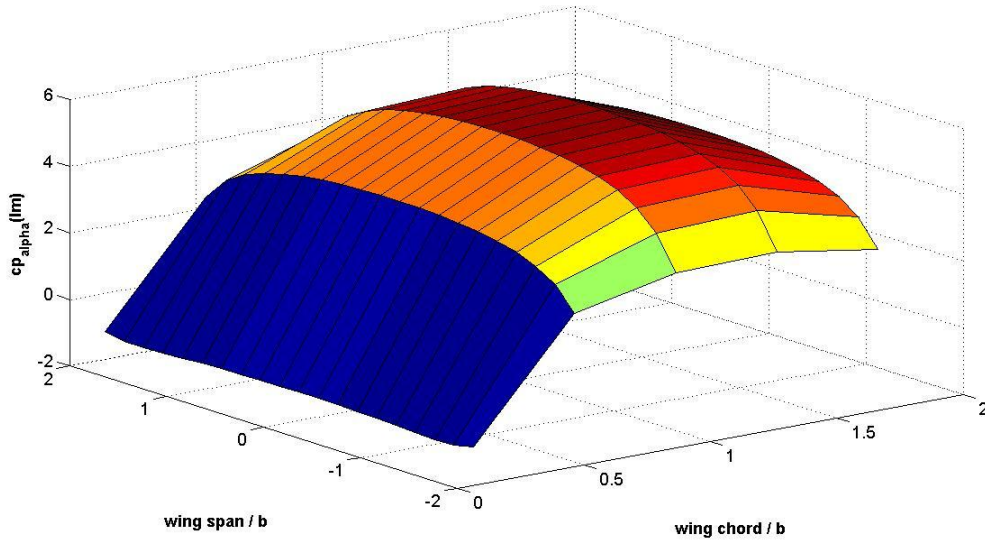
Fig. 5. Imaginary part of the pressure distribution on a rectangular wing oscillates in pitching motion (AR=2, k=1, M=0, N$_x$=5, N$_y$=10)
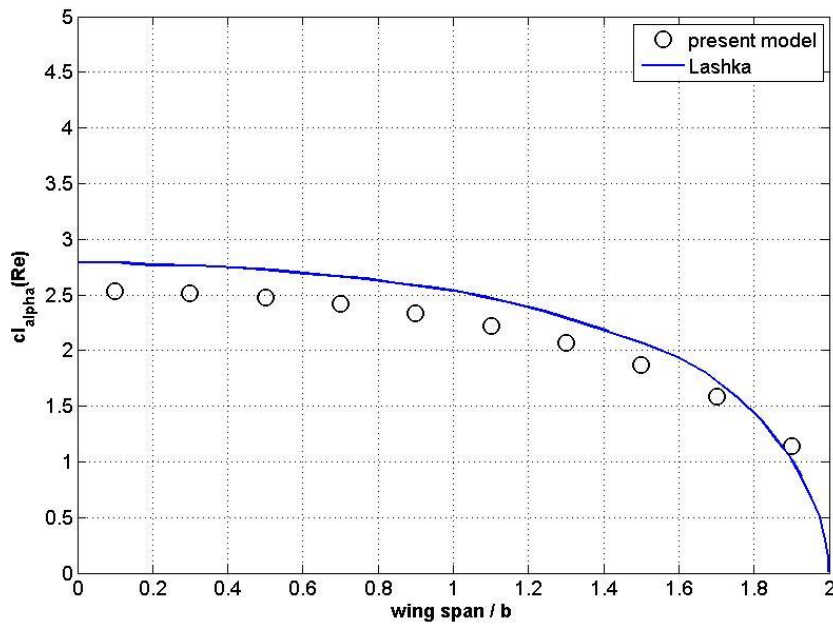
Fig. 6. Real part of the lift coefficient slope $c_{l_\alpha R}$ distribution on a rectangular wing oscillates in pitching motion (AR=2, k=1, M=0, N$_x$=5, N$_y$=10)
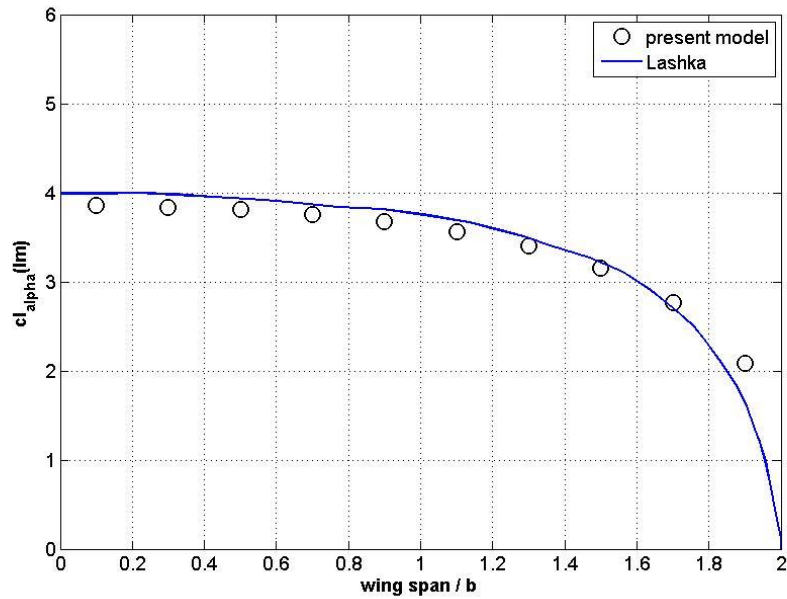
Fig. 7 Imaginary part of the lift coefficient slope $c_{l_\alpha I}$ distribution on a rectangular wing oscillates in pitching motion (AR=2, k=1, M=0, N_x=5, N_y=10)
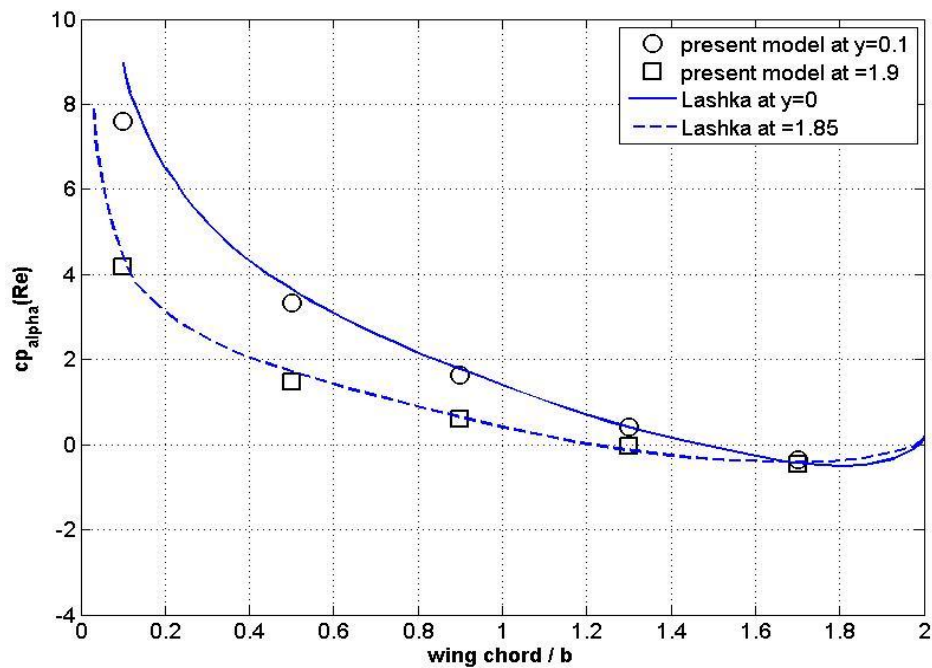
Fig. 8. Real part of the pressure coefficient $c_{p_\alpha R}$ chordwise distribution at the tip and root of a rectangular wing oscillates in pitching motion (AR=2, k=1, M=0, N_x=5, N_y=10)
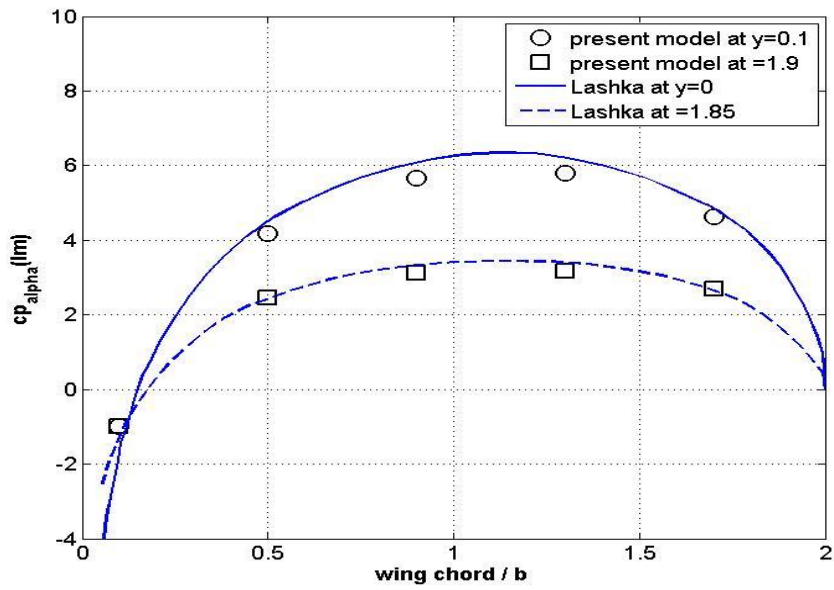
Fig. 9. Imaginary part of the pressure coefficient $c_{p_\alpha I}$ chordwise distribution at the tip and root of a rectangular wing oscillates in pitching motion (AR=2, k=1, M=0, N_x=5, N_y=10)
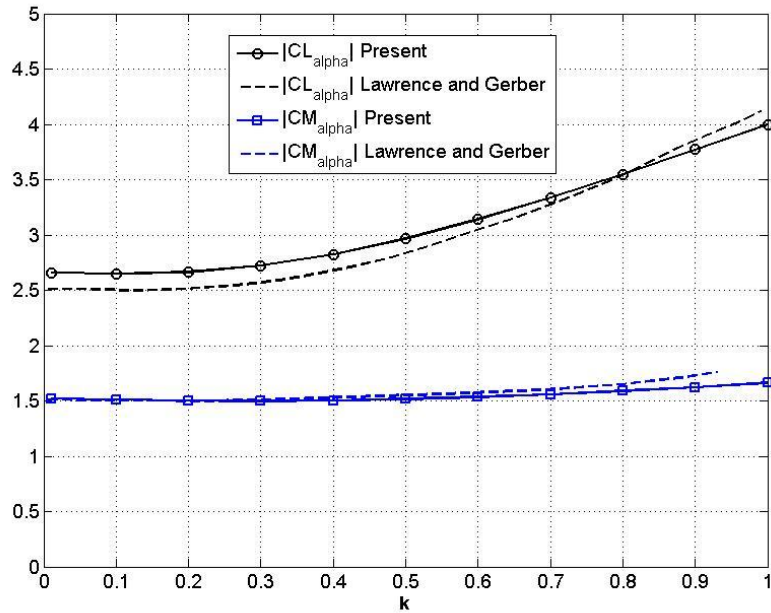
Fig. 10. The magnitude of the complex lift and moment coefficients C_L and C_M of a rectangular wing oscillates in pitching motion vs. reduced frequency

13
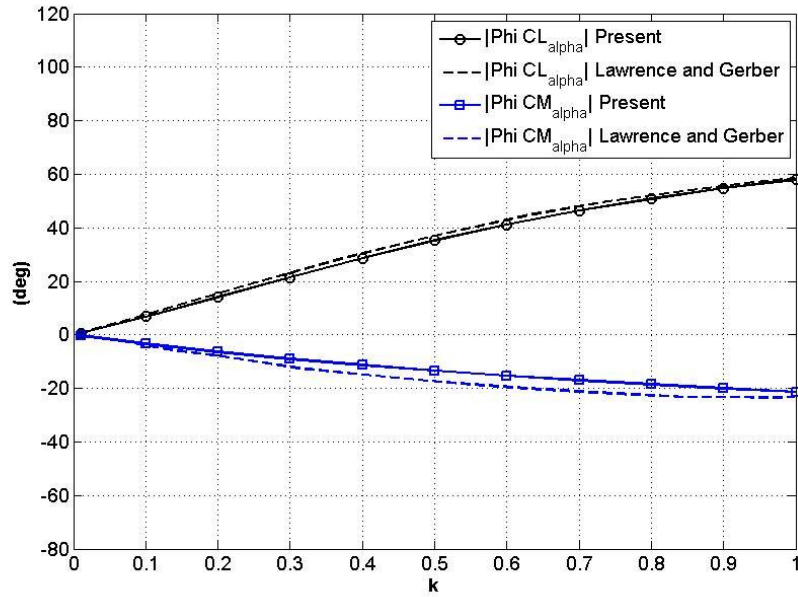
Fig. 11. The phase of the complex lift and moment coefficients C_L and C_M of a rectangular wing oscillates in pitching motion vs. reduced frequency

6.3. Aeroelastic Performance of Rectangular Composite Plate

A rectangular cantilevered composite plate is considered as a half-span representation of an aircraft wing. The plate has a length of L=12 in (0.3048 m) and a width of 2b=3 in (0.0762 m), and a thickness of t=0.804×10^{-3} m. Six layers of a unidirectional graphite/epoxy tape are used to form six different stacking sequence laminates. The material constants of the individual layers are given in Table 1, [1]. The cantilevered plates have symmetric lamination sequences as follows, $[0_2/90]_s$, $[\pm45/0]_s$, $[+45_2/0]_s$, $[-45_2/0]_s$, $[+30_2/0]_s$, $[-30_2/0]_s$.

Table 1. Engineering constants of the unidirectional graphite/epoxy tape, [1]

E_{11} [GPa]	$E_{22}=E_{33}$ [GPa]	G_{12} [GPa]	ν_{12}	Ply thickness t_p [m]	Density ρ [kg/m³]
98	7.9	5.6	0.28	0.134×10^{-3}	1520

As shown in Table 2, the present model's natural frequency results have generally good agreement with published experimental data, [1], and analytical natural frequencies calculated using 5-term Rayleigh-Ritz method.

Table 2. Natural frequencies of laminates

Laminate	Vibration mode	Experimental frequency, [Hz], [1]	Ref [1]		Present model	
			frequency, [Hz]	Δ %	frequency, [Hz],	Δ %
$[0_2/90]_s$	1B	11.1	10.7	-3.604	11.063	-0.3333
	1T	42	39	-7.143	39.747	-5.3643
	2B	69	67	-2.899	70.093	1.5841
$[\pm45/0]_s$	1B	6.1	5.7	-6.557	5.986	-1.8689
	2B	38	37	-2.632	36.758	-3.2684
	1T	77	69	-10.39	71.708	-6.8727
$[+45_2/0]_s$ $[-45_2/0]_s$	1B	4.8	4.6	-4.167	4.004	-16.583
	2B	30	32	6.6667	26.76	-10.8
	1T	51	55	7.8431	56.24	10.275
$[+30_2/0]_s$ $[-30_2/0]_s$	1B	6	6	0	6.118	1.9667
	2B	36	41	13.889	37.45	4.0278
	1T	58	60	3.4483	62.98	8.5862

The U-g and U-ω diagrams for the used cantilever plates with different stacking sequences are shown in Fig. 12 to Fig. 15. Using 9-term Rayleigh-Ritz method and 6×8 aerodynamic Doublet Points, flutter speeds (U_f) and flutter frequencies (ω_f) are determined graphically and listed in Table 3. Results are compared to experimental data, [1], analytical results calculated using 5-term Rayleigh-Ritz method, applying strip theory for the aerodynamic modeling, [1]. For further verification, two extra finite element models are considered; 3×12 FE, using Doublet Lattice method for aerodynamic model, [2], and 2×6 FE, using 6×8 Doublet Point method for aerodynamic model, [3]. The results are accurate for $[+45_2/0]_s$ and $[+30_2/0]_s$ cantilever plates, while for other stacking sequences, flutter speeds differ. It is noticeable from Fig. 12 to Fig. 15 that the bending mode is responsible for the flutter phenomenon in the plates of $[+45_2/0]_s$ and $[+30_2/0]_s$ stacking sequences, while the torsional mode is responsible for the flutter phenomenon in the other plates.

The divergence speeds (U_D) for the used lamination cantilever plates are listed in Table 4. The same theories used in flutter validation are applied. The comparison shows a good agreement in all stacking sequences.

Table 3. Flutter speed [m/s] and flutter frequencies [Hz] of laminates

	$[+45_2/0]_s$		$[-45_2/0]_s$		$[+30_2/0]_s$		$[-30_2/0]_s$	
	U_f	ω_f	U_f	ω_f	U_f	ω_f	U_f	ω_f
Experimental,[1]	28	24	div.	div.	27	28	div.	div.
Present model Rayleigh-Ritz (9 terms), Aero (Doublet Point) 6×8	23.6	21	div. 25.1	div. 48.1	25.8	28.9	div. 37.7	div. 45.2
Rayleigh-Ritz 5 terms, Aero (strip theory), [1]	27.8	28	27.8	27	27.8	31	30	29
FE 3×12, Aero (Doublet Lattice),[2]	-	-	-	-	24.9	26.4	-	-
FE 2×6, Aero Doublet Point 6×8,[3]	27.6	23.9	-	-	27.2	28	-	-
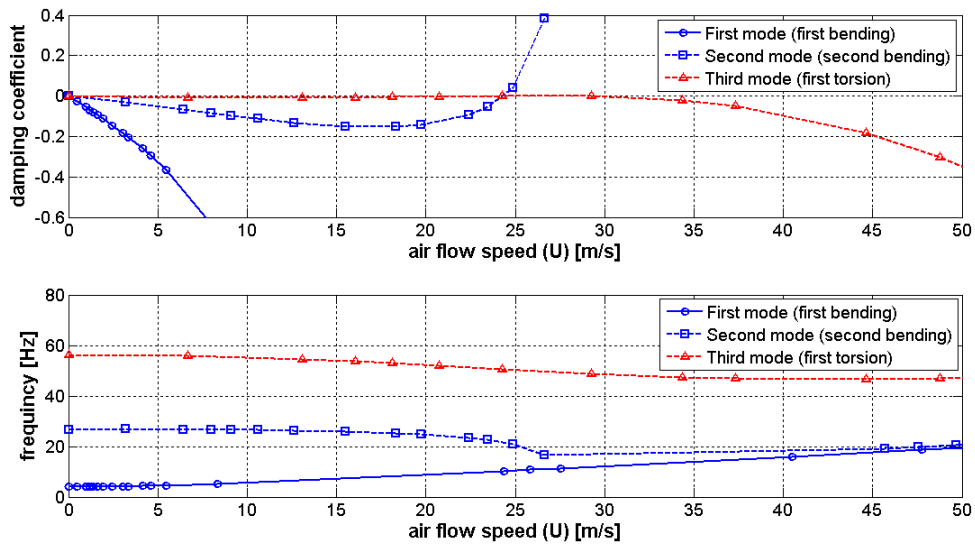
Fig. 12. The U-g curve and U-frequency curve for a [+45/0]ₛ plate wing
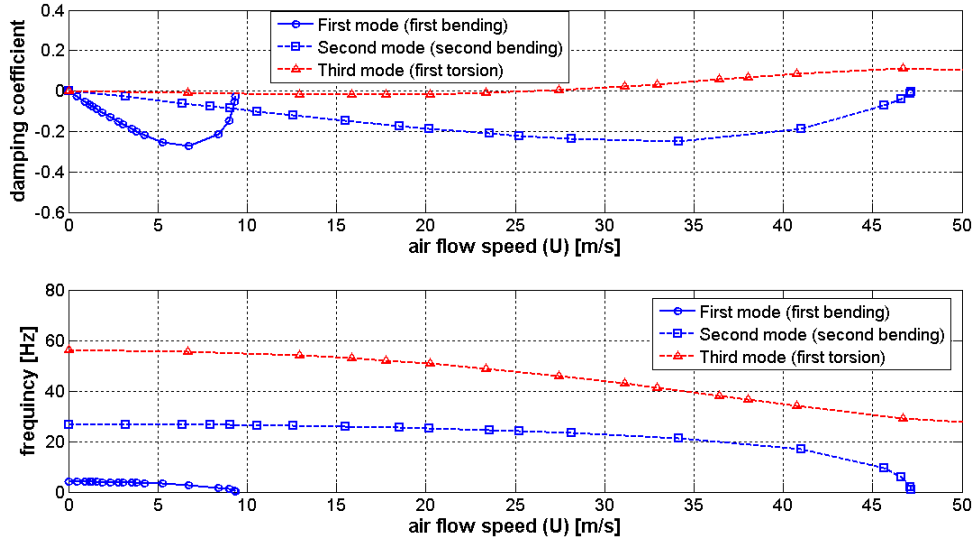
Fig. 13. The U-g curve and U-frequency curve for a [-45/0]ₛ plate wing
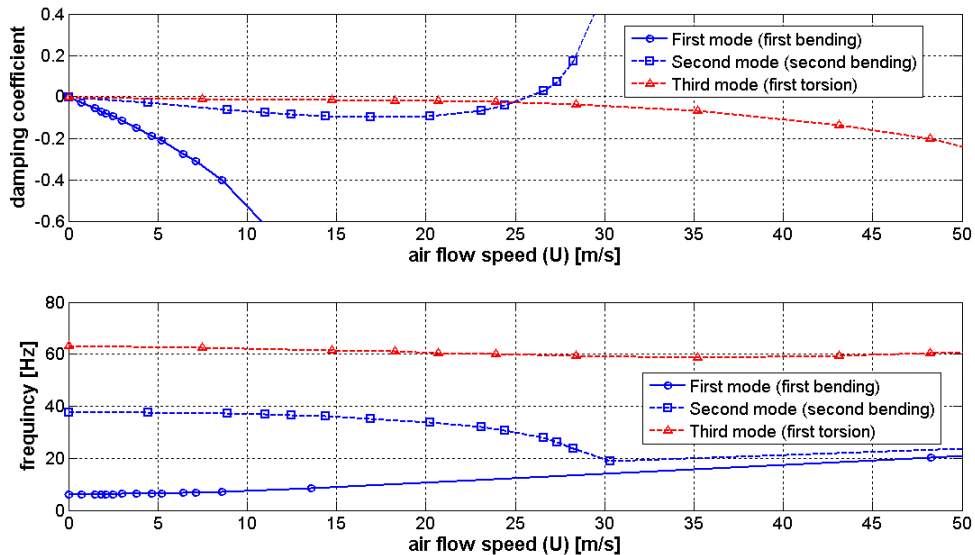
Fig. 14. The U-g curve and U-frequency curve for a [+30/0]ₛ plate wing

16
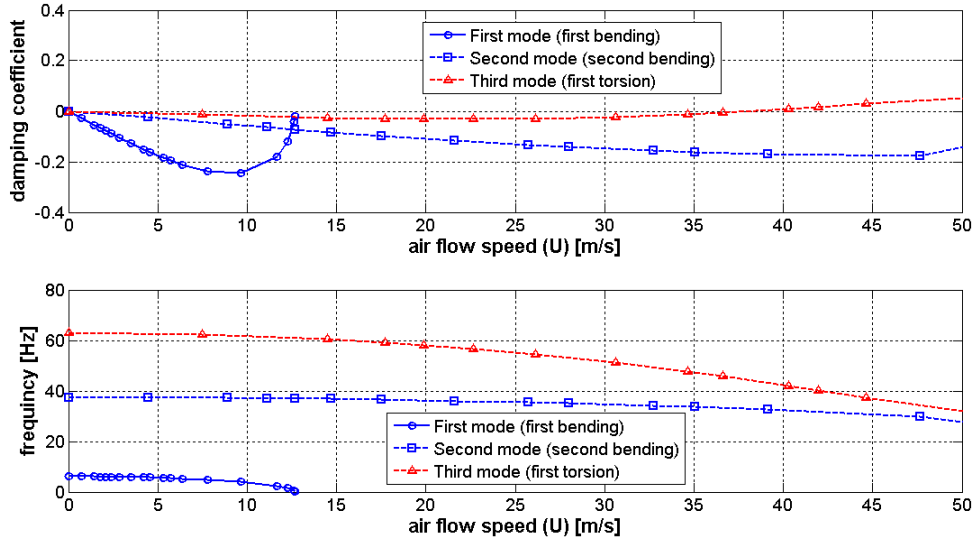
Fig. 15. The U-g curve and U-frequency curve for a [-30/0]$_s$ plate wing

Table 4. Divergence speed of laminates

	[0$_2$/90]$_s$	[±45/0]$_s$	[+45$_2$/0]$_s$	[−45$_2$/0]$_s$	[+30$_2$/0]$_s$	[−30$_2$/0]$_s$
Experimental,[1]	flutter	>32	flutter	12.5	flutter	11.7
Present model Rayleigh-Ritz (9 terms), Aero (Doublet Point) 6×8	29.13	No div.	No div.	9.125	No div.	12.33
Rayleigh-Ritz (5 terms), Aero (strip theory), [1]	22.3	infinite	infinite	9.9	infinite	10.2
Rayleigh-Ritz (5 terms), Aero (modified strip theory), [1]	25	No div.	No div.	11.1	No div.	11.5

6.4. Effect of Composite Filament Angle on Flutter and Divergence

A rectangular cantilevered composite plate is considered as a half-span representation of an aircraft wing. The plate has an aspect ratio of (AR=4), a width of (2b=1 m), and a total thickness of (t=0.016 m). The material properties of the calculated unidirectional composite plate are given in Table 5, [2].The composite fiber angle is varied in the range (-90° to 90°). Flutter and divergence speeds (U$_f$, U$_D$), flutter and natural frequencies (ω$_f$, ω$_n$) are calculated, normalized and plotted in Fig. 16 and Fig. 17 , respectively. The obtained results have good correlation with those in reference [2]. It is clear that positive fiber angles produce divergence-free wings, but the flutter speeds are small relative to negative fiber angle wings. Therefore it is difficult to obtain composite tailoring that simultaneously achieves high-flutter and high-divergence boundaries.

Table 5. Engineering constants of the unidirectional composite plate, [2]

E$_{11}$ [GPa]	E$_{22}$=E$_{33}$ [GPa]	G$_{12}$ [GPa]	ν$_{12}$	Ply thickness t$_p$ [m]	Density ρ [kg/m^3]
32	4	1.6	0.25	0.134×10^{-3}	1500
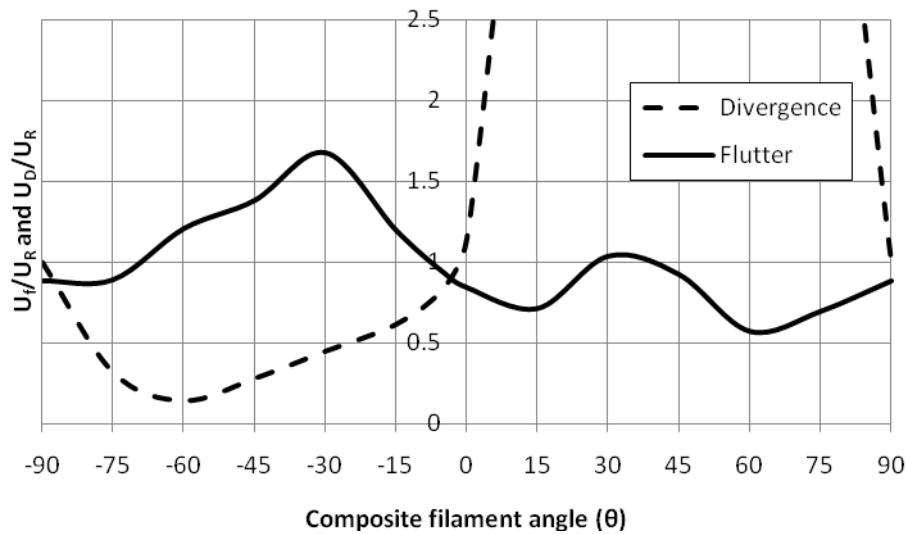
Fig. 16. Flutter and divergence speeds (U_f, U_D) normalized with respect to U_R=44.67 m/s (U_D at θ=90°)
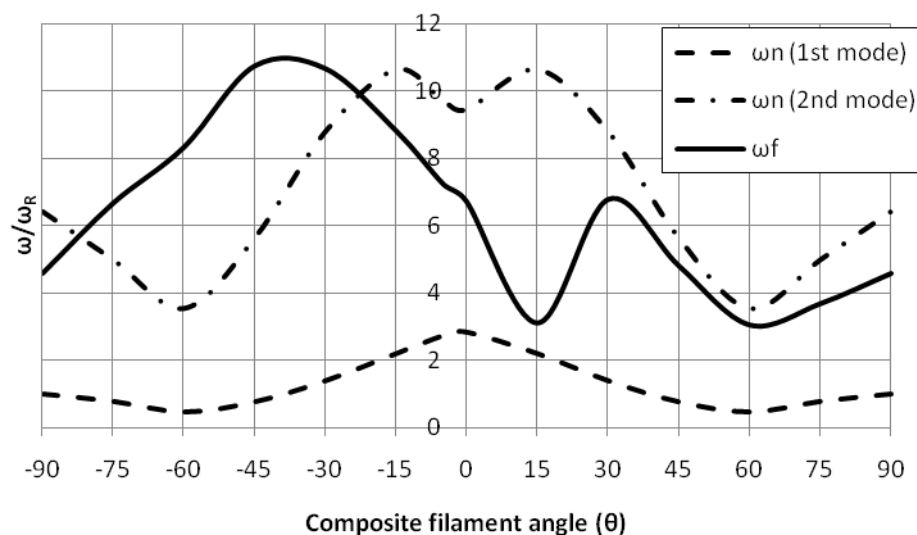
Fig. 17. Flutter and natural frequencies (ω_f, ω_n) normalized with respect to ω_R=1.665 rad/sec (1st natural frequency at θ=90°)

7. Conclusion

An analytical investigation is conducted to determine the flutter and divergence behavior of unswept, rectangular wings simulated by cantilevered composite plates with energy formulation and unsteady incompressible two-dimensional aerodynamic theory. Doublet point method was used to solve the subsonic unsteady flow over a rectangular wing. The modified higher order plate theory was used with the aerodynamic model to determine aeroelastic performance. Flutter and divergence velocities are obtained using the U-g method, and are compared to the published analytical, finite element, and wind tunnel test results and found reasonable. It is concluded that positive fiber angles produce divergence-free wings, but the flutter speeds are small relative to negative fiber angle wings. Therefore it is difficult to obtain composite tailoring that simultaneously achieves high-flutter and high-divergence boundaries.

18

8. References

[1]   S. J. Hollowell and J. Dugundji, "Aeroelastic flutter and divergence stiffness coupled, graphite/epoxy cantilevered plates," *Journal of Aircraft,* vol. 21, NO. 1, pp. 69-76, Jan 1984.

[2]   K. J. Lin, P. J. Lu, and J. Q. Tarn, "Flutter Analysis of cantilever composite plate in subsonic flow," *AIAA Journal,* vol. 27, pp. 1102-1109, 1989.

[3]   K. N. Koo and I. Lee, "Aeroelastic behavior of a composite plate wing with structural damping," *Computers & Structures,* vol. 50, No. 2, pp. 167-176, 1994.

[4]   W. G. Abdelrahmen, "Static and dynamic behaviour of composite swept wings," Master thesis, Aerospace engineering, Cairo, Giza.

[5]   P. Dunn and J. Dugundji, "Nonlinear stall flutter and divergince analysis of cantilevered graphite/epoxy wings," *AIAA Journal,* vol. 30, No. 1, pp. 153-162, January 1992.

[6]   E. Livne and W.-L. Li, "Aeroservoelastic aspects of wing/control surface planform shape optimization," *AIAA Journal,* vol. 33, No. 2, pp. 302-311, February 1995.

[7]   P.-J. Lu and L.-J. Huang, "Flutter suppression of thin airfoils using active acoustic excitations," *AIAA Journal,* vol. 30, No. 12, pp. 2873-2881, December 1992.

[8]   H. G. Kussner, "General Airfoil Theory," *NACA TM 979,* 1941.

[9]   C. E. Watkins, D. S. Woolston, and H. J. Cunningham, "A systematic Kernel function procedure for determining aerodynamic forces on oscillating or steady finite wings at subsonic speeds," *NASA TR R-48, 1959*.

[10]   W. S. Rowe M. C. Redman, F. E. Ehlers, and J. D. Sebastian, "Prediction of unsteady aerodynamic loadings caused by leading edge and trailing edge control surface motion in subsonic compressible flow- Analysis and results," *NASA CR-2543,* 1975.

[11]   E. Albano and W. P. Rodden, "A doublet lattice method for calculating lift distribution on oscillating surfaces in subsonic flows," *AIAA Journal,* vol. 7, pp. 279-285, Feb. 1969.

[12]   M. Blair, "A compilation of the mathimatics leading to the doublet lattice method," Wright Laboratory, WL-TR-92-3028, March 1992.

[13]   W. P. Rodden, Paul F. Taylor, and Samuel C. McIntosh, "Further refinement of the subsonic doublet-lattice method," *Journal of Aircraft,* vol. 35, No.5, pp. 720-727, 1998.

[14]   T. Ueda and E. H. Dowell, "A new solution method for lifting surfaces in subsonic flow," *AIAA Journal,* vol. 20, pp. 348-355, 1982.

[15]   M. Kassem Abbas, M. Adnan Elshafei, and H. M. Negm, "Modeling and Analysis of Laminated Composite Plate Using Modified Higher Order Shear Deformation Theory," presented at the 15th international conference on aerospace sience & aviation technology, ASAT-15, 2013.

[16]   E. H. Dowell, Sijthoff and Noordhoff, and Alphen aaan Rijn, *A Modern Course in Aeroelasticity*: The Netherlands, 1978.

[17]   R. L. Bisplinghoff, Holt Ashley, and Robrt L. Halfman, *Aeroelasticity*. Mineola, New York: Dover Publications, inc., 1996.

[18]   T. Ueda, "Asymptotic expansion of the kernel functionin subsonic unsteady lifting surface theory," *Journal of Japan Society of Aero/Space Sciences,* vol. 29, No.326, pp. 169-174, 1981.

Appendix (A)

Parameters used in the Eq.(6) are defined as follows, [14]:

$$x_0 = x - \zeta \qquad\qquad y_0 = y - \eta \qquad\qquad r = |y_0|$$

$$R = \sqrt{x_0^2 + \beta^2 r^2} \qquad\qquad X = \frac{(x_0 - MR)}{\beta^2} \qquad\qquad \beta = \sqrt{1 - M^2} \qquad\text{(A-1)}$$

The function $B(k,r,X)$ in the Kernel function, Eq.(6), represents an integral function of complex values:

$$B(k,r,X) = \int_{-\infty}^{X} \frac{e^{ikv}}{(v^2 + r^2)^{3/2}} dv \qquad\qquad\text{(A-2)}$$

The function $B(k,r,X)$ can be separated into two real functions as

$$B(k,r,X) = B_R(k,r,X) + iB_I(k,r,X) \qquad\qquad\text{(A-3)}$$

Values of these functions can be obtained by the series found in [18] as follows,

$$B_R(k,r,X) = \int_{-\infty}^{X} \frac{\cos(kv)}{(v^2 + r^2)^{3/2}} dv, \qquad B_I(k,r,X) = \int_{-\infty}^{X} \frac{\sin(kv)}{(v^2 + r^2)^{3/2}} dv \qquad\text{(A-4)}$$

These functions can be expressed as

$$B_R(k,r,X) = \sum_{n=0}^{\infty} (-1)^n U_{2n} - \frac{k^2}{2} \sum_{n=0}^{\infty} \frac{(kr/2)^{2n}}{(n+1)(n!)^2} \times \left\{ \sum_{m=1}^{n} \frac{1}{m} + \frac{1}{2(n+1)} - \gamma - \ln\frac{k}{2} \right\} \qquad\text{(A-5)}$$

$$B_I(k,r,X) = \sum_{n=0}^{\infty} (-1)^n U_{2n+1} + \frac{\pi}{4} k^2 \sum_{n=0}^{\infty} \frac{(kr/2)^{2n}}{(n+1)(n!)^2} \qquad\text{(A-6)}$$

where the term U_n is a function of X, and can be calculated with the aid of the recurrence formula:

$$U_n = \frac{k}{(n-2)n!} \frac{(kX)^{n-1}}{\sqrt{X^2 + r^2}} - \frac{(kr)^2}{n(n-2)} U_{n-2} \qquad (n \geq 3) \qquad\text{(A-7)}$$

The initial terms of the recurrence formula Eq.(A-7) are given by,

$$U_0 = \frac{1}{\sqrt{X^2 + r^2}\left(\sqrt{X^2 + r^2} - X\right)}$$

$$U_1 = \frac{-k}{\sqrt{X^2 + r^2}} \qquad\qquad\qquad\text{(A-8)}$$

$$U_2 = -\frac{k^2}{2}\left[\frac{X}{\sqrt{X^2 + r^2}} + \ln\left(\sqrt{X^2 + r^2} - X\right) \right]$$

When an upwash point is downstream of a doublet point, the value of the function B_R should be evaluated by [14],

$$B_R(k,r,X) \to -B_R(k,r,-X) - \frac{\pi^2}{6\sigma_j^2} + k^2\left(\ln\frac{k\sigma_j}{2} + \gamma - \frac{3}{2} \right) \quad (r < \sigma_j, X > 0) \qquad\text{(A-9)}$$

where γ is the Euler's constant $\gamma \approx 0.5772$.

Appendix (B)

The complex lift and moment coefficients can be calculated by taking the following chordwise summation at span station $y = y_j$, [14],

$$C_l\left(y_j\right) = \frac{\sum\limits_{i}^{N_x} c_{p_i}\Delta_i}{\sum\limits_{i}^{N_x}\Delta_i}, C_m\left(y_j\right) = \frac{\sum\limits_{i}^{N_x} c_{p_i}\Delta_i\left(x_m - x_i\right)}{\sum\limits_{i}^{N_x}\Delta_i} \tag{B-1}$$

The total lift and moment coefficients of the wing can be calculated by taking the following spanwise summations,

$$C_L = \frac{\sum\limits_{j}^{N_y}\left[C_l\left(y_j\right)\sum\limits_{i}^{N_x}\Delta_i\right]}{S}, C_M = \frac{\sum\limits_{j}^{N_y}\left[C_m\left(y_j\right)\sum\limits_{i}^{N_x}\Delta_i\right]}{S} \tag{B-2}$$

where S is a total wing area, and x_m the location of the axis around which the moment force is calculated.